MOTILITY ANALYSIS OF CIRCULARLY SWIMMING BULL SPERMATOZOA BY QUASI-ELASTIC LIGHT SCATTERING AND CINEMATOGRAPHY

T. CRAIG, F. R. HALLETT, AND B. NICKEL
Department of Physics, University of Guelph, Guelph, Ontario N1G 2W1 Canada

ABSTRACT The Rayleigh-Gans-Debye approximation is used to predict the electric field autocorrelation functions of light scattered from circularly swimming bull spermatozoa. Using parameters determined from cinematography and modeling the cells as coated ellipsoids of semiaxes $a = 0.5$ μm, $b = 2.3$ μm, and $c = 9.0$ μm, we were able to obtain model spectra that mimic the data exactly. A coat is found to be a necessary attribute of the particle. It is also clear that these model functions at 15° may be represented by the relatively simple function used before by Hallett et al. (1978) to fit data from circularly swimming cells, thus giving some physical meaning to these functional shapes. Because of this agreement the half-widths of experimental functions can now be interpreted in terms of an oscillatory frequency for the movement of the circularly swimming cell. The cinematographic results show a trend to chaotic behavior as the temperature of the sample is increased, with concomitant decrease in overall efficiency. This is manifested by a decrease in oscillatory frequency and translational speed.

INTRODUCTION

Ejaculates of semen from the bull contain cells exhibiting three types of motion: normally (helical) swimming cells, defective (circular) swimming cells, and dead (diffusing) cells. The first analysis of the motion of defective cells from these ejaculates was undertaken by Rikmenspoel et al. (1960), who made cinematographic measurements of the frequency and amplitude of the tail wave as well as of the progressive swimming speed. He found no definite relationship between the swimming speed and the frequency of the tail wave. Many light scattering experiments have been undertaken on the spermatozoa of the bull (Cooke et al., 1976; Hallett et al., 1978; Craig et al., 1979; Shimizu and Matsumoto, 1980) and human (Adam et al., 1969; Dubois et al., 1975). Of these studies only Hallett et al. (1978) included the defective population in their analysis. They found that by using the speed distribution, $P_s(v)$,

$$P_s(v) = \frac{1}{4\pi\bar{v}} e^{-v/\bar{v}}, \tag{1}$$

and a point scattering model developed by Nossal (1971), they could produce an expression for the electric field autocorrelation function, $g^1(\tau)$, which fit experimental functions obtained from defective cells. This function has the form

$$g^{(1)}(\tau) = \frac{1}{k\bar{v}_c\tau} \tan^{-1}(k\bar{v}_c\tau), \tag{2}$$

where k is the magnitude of the scattering vector, τ the experimental delay time, and $\bar{v}_c$ the average speed of the particles. With this procedure it was possible to determine the fraction of defective cells in the ejaculate as well as their average swimming speed. However, the assumption that spermatozoa behave as point particles is difficult to reconcile with their actual dimensions, which are somewhat larger than the wavelength of light used. Indeed, Craig et al. (1979) demonstrated that normal spermatozoa were better modeled as ellipsoid Rayleigh-Gans-Debye scatterers of semiaxes 0.5 μm × 2.3 μm × 9.0 μm. In this paper we shall provide a similar analysis of defectively swimming cells. Results indicate that the properties of experimental electric field autocorrelation functions are determined primarily by the oscillatory movements of the heads of these cells and not by their progressive speeds, thus changing the interpretation of the half-widths obtained by Hallett et al. (1978).

THEORY

The trajectory of the motion of the defective cell is somewhat different than the helical motion of the normal cell. During the defective motion, the head of the spermatozoon traces out a roughly sinusoidal path about its circular track with some in-phase tilting about the long axis of the cell out of the plane of the path (Fig. 1). The parameters necessary to specify this trajectory are the frequency of this sinusoidal movement (ω), the maximum tilt angle of the head (β_0), the maximum out-of-plane tilt (γ_0), the maximum displacement of the head from the line of motion (R_0) and the speed (v). The angular frequency ω is distinct from the tail beat frequency.

It will be assumed that the spermatozoon can be modeled as an ellipsoid of semiaxes a, b, and c, with its centre of mass undergoing a sinusoidal motion about its direction of forward motion.

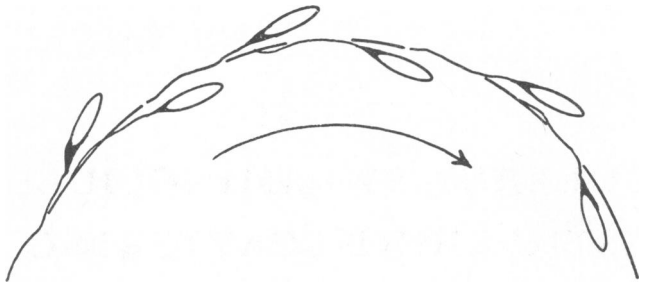

FIGURE 1 Trajectory of the motion of a circularly swimming bull spermatozoon cell. The overall path is denoted by the dashed line.

The general equation for the electric field autocorrelation function of such a motile particle is (Craig et al., 1979; Holz and Chen, 1978)

$$g^{(1)}(\tau) = C_N^{-1}\left\langle \frac{1}{4\pi}\int_0^{2\pi} d\psi_0 \int_{-1}^{+1} d\nu e^{jk\nu\tau}\, e^{j\mathbf{k}\cdot[\mathbf{R}(\tau)-\mathbf{R}(0)]} A(\mathbf{k},\tau)A^*(\mathbf{k},0)\right\rangle, \quad (3)$$

where C_N is a normalization constant, τ is delay time, $\mathbf{R}(\tau)$ is the component of the position of the particle parallel to the **a** axis, ψ gives the orientation of the **a** axis in the x-y plane, $\nu = \cos\theta$ is the orientation of the scattering vector **k**, which is arbitrarily placed in the x-z plane. The direction of motion is along the z axis (Fig. 2). $A(\mathbf{k},\tau)$ is the form factor for the particle, which depends on its overall shape and orientation with respect to the scattering vector **k**, and is described by

$$A(\mathbf{k},\tau) = 3j_1(K)/K, \quad (4)$$

where

$$K^2 = (\mathbf{k}\cdot\mathbf{a})^2 + (\mathbf{k}\cdot\mathbf{b})^2 + (\mathbf{k}\cdot\mathbf{c})^2. \quad (5)$$

The angle brackets in Eq. 3 indicate averaging over dynamic quantities, such as the frequency of motion of the particle. One assumption inherent in Eq. 3 is that the particle travels in straight lines for long times compared with $(kv)^{-1}$. This assumption will be shown to be appropriate later, when cinematographic data are shown.

The motion of the centroid of the particle is displaced from the average direction of motion, the z axis, by a distance **R** (Eq. 3). Since **R** was defined earlier as being parallel to **a** (Craig et al., 1979), it is necessary to make **b** the small semiaxis. The sinusoidal motion is then described as a rotation about **b** by the angle

$$\beta = \beta_0 \sin(\omega\tau + \delta_0), \quad (6)$$

with a concomitant sinusoidal variation of R, given by

$$R = R_0 \sin(\omega\tau + \delta_0). \quad (7)$$

Now, as R_0 is defined as the maximum displacement of the centroid when β is a maximum,

$$R_0 = X \sin\beta_0, \quad (8)$$

where X is defined as the displacement of the point of rotation from the centroid along the **c** axis as described in Fig. 3. The out-of-plane motion is described by a rotation about **c** by the angle

$$\gamma = \gamma_0 \sin(\omega\tau + \delta_0). \quad (9)$$

The appropriate dot products required for Eqs. 3 and 5 in this case are

$$\mathbf{k}\cdot\mathbf{R} = Rk\cos\psi\sin\theta, \quad (10a)$$

$$\mathbf{k}\cdot\mathbf{a} = ak[(\cos\gamma\cos\beta\cos\psi - \sin\gamma\sin\psi)\sin\theta - \cos\gamma\sin\beta\cos\theta], \quad (10b)$$

$$\mathbf{k}\cdot\mathbf{b} = bk[-(\sin\gamma\cos\beta\cos\psi + \cos\gamma\sin\psi)\sin\theta + \sin\gamma\sin\beta\cos\beta], \quad (10c)$$

$$\mathbf{k}\cdot\mathbf{c} = ck(\sin\beta\cos\psi\sin\theta + \cos\beta\cos\theta). \quad (10d)$$

$A(\mathbf{k},\tau)$ from Eq. 4 is periodic in the variable δ, and can be described by a Fourier series (Craig et al., 1979):

$$\langle A(\mathbf{k},\tau)A^*(\mathbf{k},0)\rangle_{\delta_0} = \sum_n |B_n|^2 e^{jn\omega\tau}. \quad (11)$$

This simplifies Eq. 3 to

$$g^{(1)}(\tau) = C_N^{-1}\left\langle \frac{1}{4\pi}\int_0^{2\pi} d\psi_0 \int_{-1}^{+1} d\nu e^{jk\nu\tau} \sum_n |B_n|^2 e^{jn\omega\tau}\right\rangle. \quad (12)$$

Further simplification can be achieved from the following symmetries for

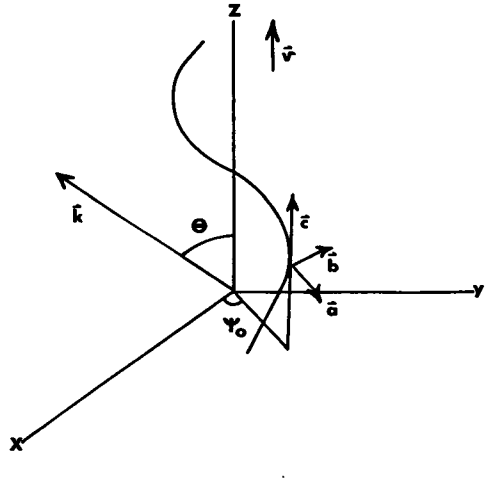

FIGURE 2 The orientation of the cell with respect to the scattering geometry.

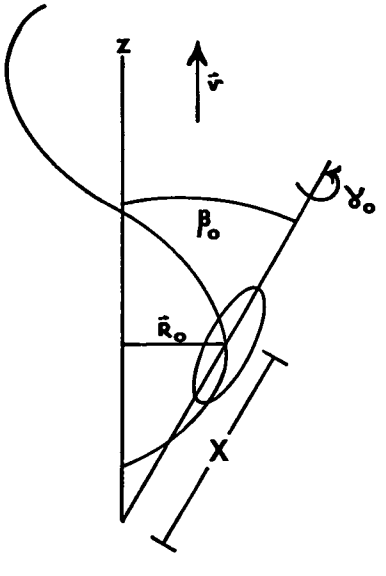

FIGURE 3 Tilt angles β_0 and γ_0 of the cell as well as the displacements R_0 and X, with respect to the overall direction of motion.

the B_n:

$$B_n(\cos\theta, \psi) = B_n(\cos\theta, -\psi), \quad (13a)$$

$$B_n(-\cos\theta, \psi) = B_n^*(\cos\theta, \psi), \quad (13b)$$

yielding

$$g^{(1)}(\tau) = C_N^{-1}\left\langle \int_0^{\pi} d\psi_0 \int d\nu\, Re(e^{ik\nu v\tau}) \sum_n Re(e^{in\omega\tau})\, B_n B_n^* \right\rangle. \quad (14)$$

Three different sets of frequency and speed distributions were used to determine the averages in Eq. 14:

$$P(v) \sim e^{-(v/\bar{v})}, \quad (15a)$$

$$P(\omega) \sim e^{-(\omega/\bar{\omega})}, \quad (15b)$$

from Hallett et al. (1978);

$$P(v) \sim v^2 e^{-(3/2)(v^2/\bar{v}^2)}, \quad (16a)$$

$$P(\omega) \sim \omega^2 e^{-(3/2)(\omega^2/\bar{\omega}^2)}, \quad (16b)$$

from Berne and Nossal (1974); and finally

$$P(v) = e^{-[(v-\bar{v})^2/2\sigma_v^2]}, \quad (17a)$$

$$P(\omega) = e^{-[\omega-\bar{\omega})^2/2\sigma_\omega^2]}. \quad (17b)$$

If Eqs. 15a and b are used in Eq. 14, the following $g^{(1)}(\tau)$ results:

$$g^{(1)}(\tau) = \sum_n \int_0^1 d\nu \int_0^{\pi} d\psi_0 [1 + p^2]^{-1} [1 + q^2]^{-1} B_n B_n^*, \quad (18)$$

where $p = k\bar{v}\nu\tau$ and $q = n\bar{\omega}\tau$. The use of Eqs. 16a and b result in

$$g^{(1)}(\tau) = \sum_n \int_0^1 d\nu \int_0^{\pi} d\psi_0 \left(1 - \frac{p^2}{2}\right) e^{-(p^2/4)} \left(1 - \frac{q^2}{2}\right) e^{-(q^2/4)} B_n B_n^*, \quad (19)$$

where $p = k\,2\overline{v^2}/3$ and $q = n\,2\overline{\omega^2}/3$.

Using Eqs. 17a and b is somewhat more complicated, because both v and ω must be defined over the interval $-\infty$ to $+\infty$. A negative v or ω is meaningless. If, however, $\bar{v}$ and $\bar{\omega}$ are sufficiently large and the respective widths of the distributions are sufficiently small, negligible amounts of these distributions exist below zero, so that this does not become a problem. Doing this gives

$$g^{(1)}(\tau) = \sum_n \int_0^1 d\nu \int_0^{\pi} d\psi_0 \cos(n\bar{\omega}\tau) \cos(k\nu\bar{v}\tau)\, e^{-(k^2\nu^2\tau^2\sigma_v^2/2)}\, e^{-(n^2\tau^2\sigma_\omega^2/2)}\, B_n B_n^*. \quad (20)$$

When $R = 0$ and $X = 0$, one has the simple case where the centroid does not move off axis and the particle exhibits an oscillatory movement about the centroid.

A coat with arbitrary thickness and index of refraction may be added to the particle by using the scheme given by Chen et al. (1977).

METHODS

Experimental

The cinematography was recorded by a Locam, 16-mm high-speed motion picture camera (model 51, Redlake Corp., Campbell, CA), mounted on a Zeiss microscope (model KL14, Carl Zeiss, Inc., New York), on black-and-white 400 ASA film (Eastman Kodak Co., Rochester, NY, 4× reversal film 7277). All the microscopy was done through a ×25 phase contrast objective, with no eyepiece optics on the camera, and

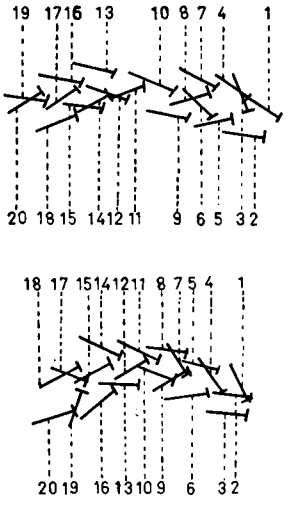

FIGURE 4 Two examples of tracings of head positions for successive frames. The numbers indicate the frame numbers. The long line lies along the midline of the length of the head with the cross bar the dividing line between the end of the head and the midpiece. Both of these were taken at ~50 frames/s.

on slides prewarmed to 30°C. Various film speeds were used. These were accurately determined from 100-s^{-1} timing marks on the film. The films were analyzed frame by frame on a data-analyzing projector (model 224A special, L-W International, Woodland Hills, CA). The position and orientation of the head of each cell studied was recorded for successive frames on acetate sheets (Fig. 4). The path of the cell for several frames was estimated and the maximum tilt angle (β_0) of the cell determined. In addition, by plotting the maximum displacement of the proximal end of the cell head as a function of time (Fig. 5), it was possible to ascertain the frequency of oscillation of the head of the spermatozoon. The progressive speed of the cell was determined by measuring the length of the track and then by using one head length as being 9.0 μm (van Duijn and van Voorst, 1971) to obtain the absolute scale. When we checked this with our cells, using a reticle on the microscope stage, the result was found to be the same.

The equipment used to determine the electric field autocorrelation function of the scattered light has been described elsewhere (Hallett et al., 1978).

The semen samples were obtained fresh from United Breeders, Inc., Guelph, Ontario and used within one hour of collection. All samples were

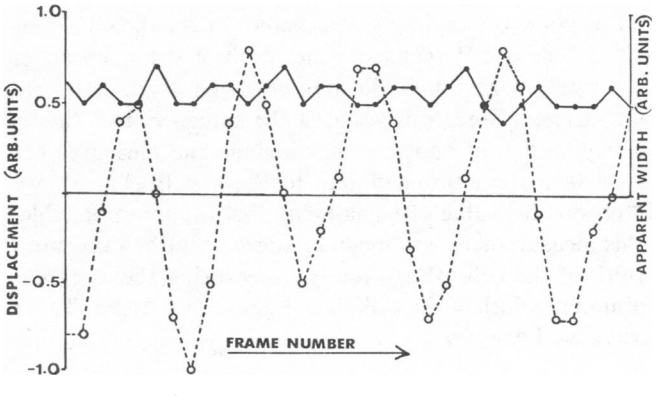

FIGURE 5 Displacement (in arbitrary units) of the proximal end of the head of the cell from the overall direction of motion as a function of frame number (○). Apparent width of the cell as a function of frame number (●).

from Holstein Friesen bulls. The cells were diluted in Hanks' balanced salt solution (HBSS) (Gibco Laboratories; Grand Island Biological Co. Inc., Grand Island, NY) by a final factor of 750. This was done in two steps. First, 0.1 ml of raw semen was diluted in 5 ml of HBSS. The cinematography was done at this dilution. Second, 1 ml of this was put in 15 ml of HBSS to obtain the final concentration of cells for the light scattering. These dilutions were performed after the sample had been transported to our laboratory. If the dilutions were performed at the site of collection, the number of circularly swimming cells was greatly reduced.

The sample was examined microscopically to ascertain whether a large number of the motile cells were circular swimmers (>95%). If this was not the case, the pH was adjusted to ~7.8 to induce the cells to swim circularly. All the glassware was kept at 30°C, as well as the scattering chamber. As these cells tend to die rather quickly, it is necessary to do the experiments as soon as possible after dilution.

Numerical

The numerical calculations to obtain the theoretical electric field autocorrelation functions were done on an Amdahl 470V/5 computer (Amdahl Corp., Sunneyvale, CA). Both the ψ and ν integrals in Eqs. 18–20 were done according to Simpson's rule with 50 segments. It was found that this number was required to give results accurate to four digits. Increasing the number of segments gave no increase in the accuracy. The details of the calculations of the Fourier coefficients and the form factor appear elsewhere (Craig et al., 1979).

RESULTS

Cinematography

By examining Fig. 4, one can see that the cell maintains the same average direction of motion for relatively long periods of time. Tracks similar to those in Fig. 4 were analyzed for 50 cells. It was found that the average speed of the cells around the circular path was 92.6 ± 30.4 (SD) μm/s at 30°C, which is somewhat higher than the ~65 μm/s found by Rikmenspoel et al. (1960) at 37°C. The frequency of the oscillatory motion was found to be 14.4 ± 2.63 Hz. The maximum angle of tilt of the head from the direction of motion (β_0) was found to be 51.3 ± 12.8° (SD). Owing to the finite resolution of the camera, this value of β_0 will be somewhat of an underestimation of the true value, since the likelihood of making the measurement at the very extreme of the motion is small. The out-of-plane tilt angle (γ_0) was determined to be 48 ± 6.6° (SD). This is different from the result of Rikmenspoel et al. (1960), who found the motion to be completely two dimensional. Since this value of the standard deviation is purely statistical and does not include the measurement error (a systematic error due to the cell thickness), we interpret this value of γ_0 as being the minimum possible. This measurement was made by measuring the maximum width of the cell (W_{max}) and by measuring the apparent minimum width of the cell (W_{min}) at another frame. These are related to γ_0 by

$$\cos \gamma_0 = \frac{W_{min}}{W_{max}}. \tag{21}$$

This value has the same inherent error in it as the measurement of β_0. In addition, since γ_0 has to be 60° for W_{min} to be half of W_{max}, there is a limitation on these measurements because of the relatively small size of the image to be measured.

Fig. 5 also contains a plot of the apparent width of the cell as a function of frame number. From this it is possible to see that β_0 and γ_0 are in phase, since when the head is at its maximum position (β_0 maximum) the apparent size is smallest (γ_0 maximum).

As shown in Fig. 6, the frequency of the oscillatory motion is completely unrelated to the speed of the forward motion. This conclusion is reinforced by a regression coefficient of only 0.007.

Cinematography was performed on a sample of circularly swimming cells at two different temperatures, room temperature (23°C) and 30°C. The average speed, $\bar{v}$, was significantly lower at 30°C than at room temperature (0.025 significance level), the average oscillatory frequency ($\bar{f}$) was also lower at 30°C (0.001 significance level) and the maximum angle (β_0) was significantly larger at 30°C (0.001 significance level). This trend is consistent with that of Rikmenspoel et al. (1960), who found an average speed of 65 μm/s at 37°C.

Light Scattering

As has been shown before (Hallett et al., 1978) and is reaffirmed here in Fig. 7, a function of the form

$$g^{(1)}(\tau) = (k\bar{v}_c\tau)^{-1} \tan^{-1}(k\bar{v}_c\tau) \tag{22}$$

represents the data from circularly swimming cells very well. Here, $\bar{v}_c$ is really related to $\bar{\omega}l$, where $\bar{\omega}$ is the angular frequency and l some characteristic length. This function

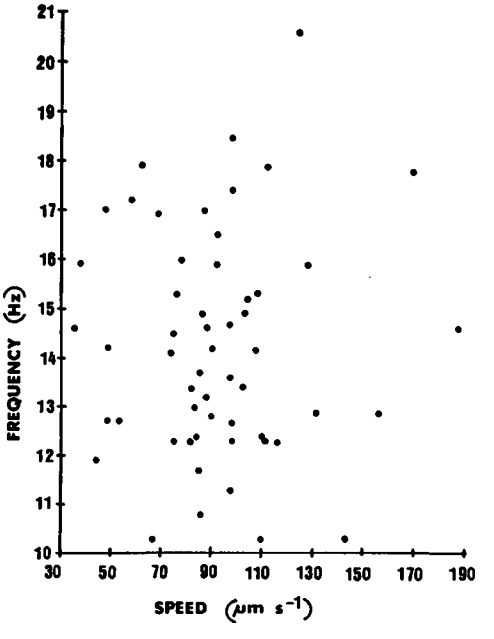

FIGURE 6 Plot of frequency vs. speed for 56 sperm cells.

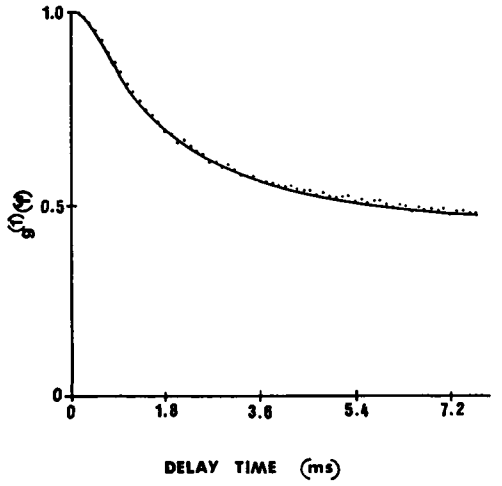

FIGURE 7 A comparison of an experimental electric field autocorrelation function for circularly swimming cells (· · ·) and a fit using Eq. 22.

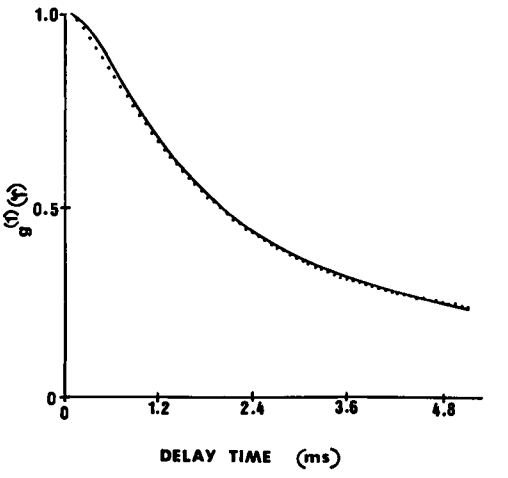

FIGURE 9 A comparison of a function representing the data from circularly swimming cells (Eq. 22) (—) and a model function calculated using Eq. 19 (· · ·).

will be used for comparison with the model calculations in subsequent figures.

The two exponential distributions (Eqs. 15a and b) were first used in Eq. 18 to calculate the model function shown in Fig. 8. The parameters used in the model calculations to match the half-width are not reasonable ones. In addition, the function does not exhibit the characteristic motile shoulder observed in all data.

The properties of Eq. 19 were investigated with the out-of-plane rotation initially set to zero (i.e., $\gamma_0 = 0$). Since the experimental half-width of a function at a scattering angle of 15° was usually ~2.0 ms, the strategy was to vary the dynamic parameters of Eq. 19 to match this half-width, as well as the shape of the data. The dynamic parameters (speed, frequency, and maximum angles) were varied within limits established by the cinematographic analyses. The static parameters (ellipsoid size) have been fixed by Craig et al. (1979) and should remain unchanged, since circularly swimming cells appear morphologically identical to normals.

The displacement X (see Fig. 3) of the centroid of the ellipse was estimated from cinematographic data to be 13 μm. This was assumed to be the maximum possible. The maximum angle β_0 was fixed at a very conservative 40°. With $a = 2.3$ μm, $b = 0.5$ μm, $c = 9.0$ μm, and the average speed set at 65 μm/s, it was necessary to have an average frequency of 35 Hz to attain a half-width of 2.0 ms. Although this frequency is more than a factor of 2 too large, the shapes of the data and model functions agree quite well as can be seen in Fig. 9. It was thought that increasing the average speed might narrow the function, which would allow the average oscillatory frequency to be reduced. As shown in Fig. 10, however, the half-width is only a weak function of the speed. Since the addition of out-of-plane motion tends to decrease the half-width of the model autocorrelation functions, reasonable values of γ_0 were then included in the calculation.

The histograms for the frequency and speed determined by cinematography are shown in Figs. 11 and 12, respec-

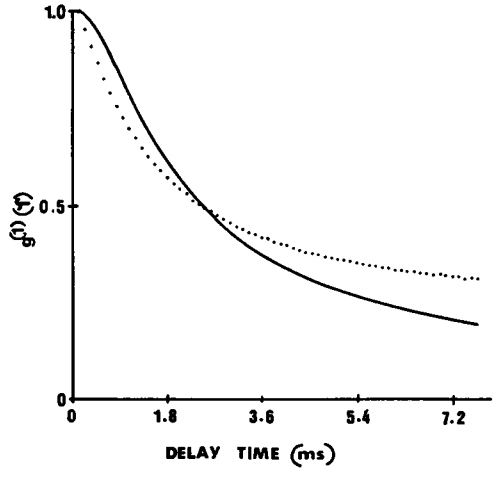

FIGURE 8 A comparison of a function representing the data from circularly swimming cells (Eq. 22) (—) and a model function calculated using Eq. 18 (· · ·).

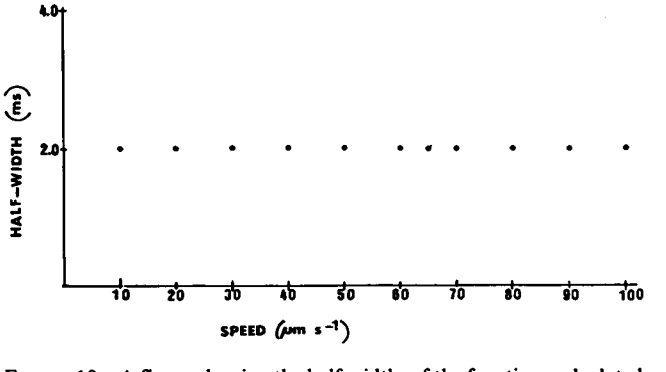

FIGURE 10 A figure showing the half-widths of the functions calculated using Eq. 19 as a function of speed. There is almost no dependence on the speed of the particle.

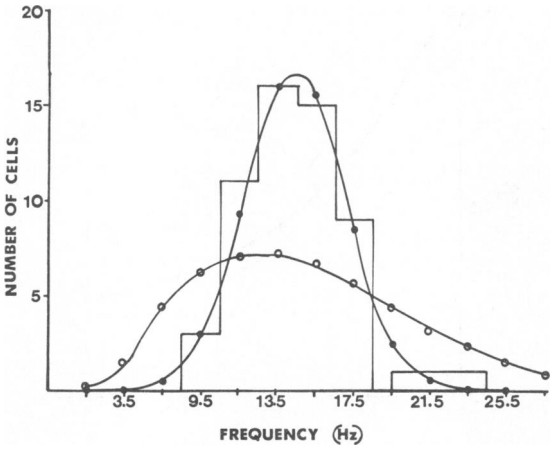

FIGURE 11 A histogram of the frequencies of the oscillatory movement of 56 circularly swimming cells. A distribution corresponding to Eq. 16a (O) and a distribution corresponding to Eq. 17a (●). The areas under the curves have been normalized to the same values.

tively. It is obvious that the distributions of Eqs. 16a and b do not approximate the true distributions as well as Eqs. 17a and b. It was therefore concluded that the features of the autocorrelation function calculated with Eq. 20 (which was determined from Eqs. 17a and b) should be examined. The size parameters were set as before. Distribution widths from cinematographic data were inserted into Eq. 20. β_0 was set at 50°, and at first γ_0 was also set to this value to correspond with the cinematographic data. The parameter R_0 was varied to get the appropriate half-width for the data. The variation of half-width with R_0 is shown in Fig. 13. The most appropriate value of R_0 was found to be 6.8 μm, which is clearly outside of the value measured by cinematography. As shown in Fig. 14, however, the shape of the model correlation function is not the same as the data. Since the discrepancies exist in the large and small times, it was thought that increasing the width of the

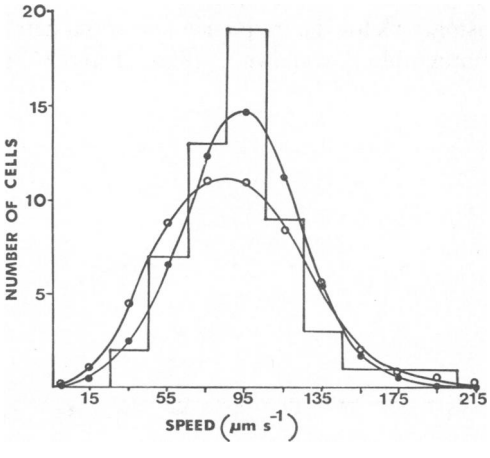

FIGURE 12 A histogram of the speeds of the circularly swimming cells. A distribution corresponding to Eq. 16b (O) and a distribution corresponding to Eq. 17b (●). The areas under the curves have been normalized to the same values.

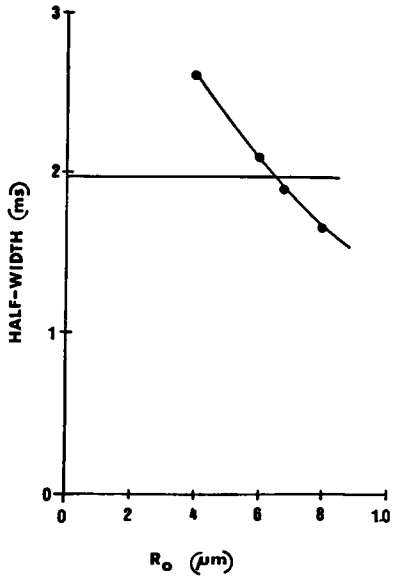

FIGURE 13 Figure showing the half-widths of functions calculated using Eq. 20 as a function of R_0.

frequency distribution might correct this. There is some justification for this since (*a*) there is a natural selection against choosing cells that are oscillating very slowly (for example, it is often hard to distinguish slow cells from those attached to a glass surface), and (*b*) any discrepancies between the actual motion and model motion would most likely appear in the high end of the frequency histogram and might not be detected at the film speed used. The increased width produced a function with somewhat better agreement than before, although not as good as was hoped.

Since the fits described above were judged to be unacceptable, a coat was added to the particle. In the case of the normal cells it was found by Craig et al. (1979) that a coat had no effect on the functions obtained at low scattering angle (~15°). This, however, is not the case with the circularly swimming cells. If the values of the thickness

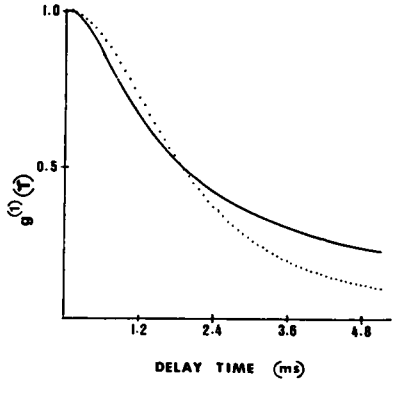

FIGURE 14 A comparison of a function representing the data (Eq. 22) (—) and a function calculated using Eq. 20 (· · ·). This particle has no coat, and σ_v and σ_ω were chosen from the cinematographic data.

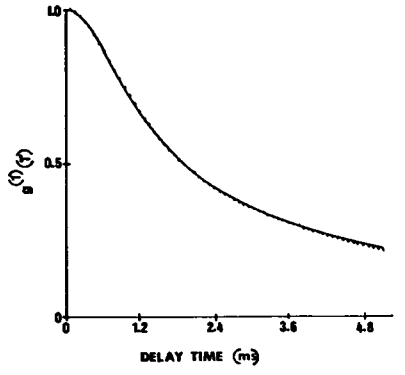

FIGURE 15 A comparison of a function representing the data from circularly swimming cells (Eq. 22) (—) and a function calculated using Eq. 20 (· · ·). This particle has a coat of index of refraction 1.44 with a thickness of 0.15 μm and an interior index of refraction of 1.33.

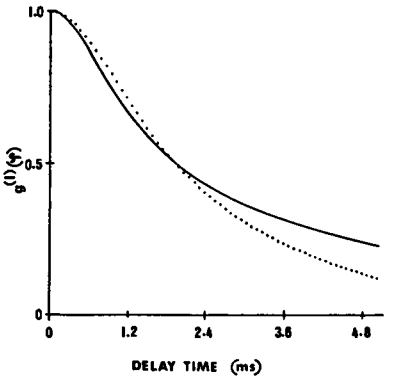

FIGURE 17 A comparison of a function representing the data from circularly swimming cells (Eq. 22) (—) and a function calculated using Eq. 20 (· · ·). This particle has a coat of thickness 0.15 μm with an index of refraction of 1.42. The interior index of refraction is 1.35. R_0 has a value of 2.77 μm and γ_0 a value of 71.7°.

of the coat, the interior index of refraction, and the coat index of refraction are varied systematically, it is found that values of 0.15 μm, 1.33, and 1.44, respectively, give the lowest difference of squares between Eq. 20 and a function of equal half-width generated from Eq. 22. This is shown in Fig. 15. These values of the thickness of the coat and the indices of refraction are questionable, although the coat thickness can be rationalized since the sperm cell is covered at the proximal end by a thick acrosome. The thickness of 0.15 μm probably corresponds to the thickness of the coat, averaged over the whole cell. If the refractive indices are altered to their experimental values (van Duijn and van Voorst, 1971), 1.35 for the interior and 1.42 for the thin coat, a slightly poorer fit is obtained (Fig. 16). Nevertheless, this fit was felt to be acceptable because the main discrepancy occurs in the long time region, near background and where the statistical quality of the experimental functions are poorest.

There still remains the problem that the value of R_0 is much larger than that measured. Using the compromise coat of 0.15 μm, if R_0 is given the measured value of 2.8 μm and γ_0 in Eq. 20 is varied until the appropriate value of the half-width is obtained, one finds that a value of 71.7° is required (Fig. 17). Angles as large as this cannot be measured from the cinematographic data. Even if the particle were perpendicular to the observer, an apparent width of 1.0 μm would be measured, which, according to the scheme of Eq. 21, would yield ~77° for γ_0. It is because of this ambiguity, the fact that the measurement of γ_0 is less accurate than the measurement of R_0, owing to the measurement technique, and the fact that the value of γ_0 is underestimated because of the finite resolution of the film that a value of 71.7° is not considered unreasonable.

Further evidence from the k-scaling behavior of these functions (Craig and Hallett, 1982) shows that if γ_0 has a value of ~50°, the peaks seen in the model k-scaling curves disappear. But these peaks are present in the experimental curves. Hence, the measured value of 50° is suspect.

The disagreement between the data and model in Fig. 16 may be due to the fact that the model used here does not properly take into account the acrosomal region of the cell, thus yielding a different line shape, as was seen when the coat was originally added (see Figs. 14 and 15). The region in the scaling curves where this is of most importance is in the region of the first peak, which may well overlap with a scattering angle of 15°, where the work presented here was done. This means that a change in R_0 to a value higher than that measured compensates for the errors in the model.

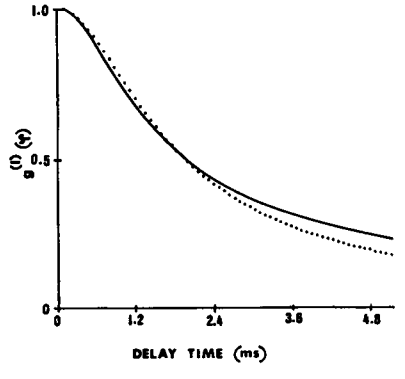

FIGURE 16 A comparison of a function representing the data from circularly swimming cells (Eq. 22) (—) and a function calculated using Eq. 20 (· · ·). This particle has a coat of index of refraction 1.42 with a thickness of 0.01 μm and an interior index of refraction of 1.35.

CONCLUSIONS

It is possible, using the Rayleigh-Gans-Debye approximation, to model the electric field autocorrelation function of light scattered from circularly swimming bull spermatozoa. This is not surprising, since it has been shown by Craig et al. (1979) that this technique works well for the normal cells. Also, Kotlarchyk et al. (1979) showed that

the Rayleigh-Gans-Debye approximation was a good one at small scattering angles, where this work was done. Moreover, it was necessary to coat the particle to obtain agreement between the model function and the data. The Rayleigh-Gans-Debye criterion is easily met for the coat, which seems to be a very important part of the scattering. It is also necessary to have a displacement of the particle from the axis larger than that measured in order to have the line shapes of the data and model agree. This appears to be due to imprecision in the model particle with respect to the acrosomal region of the cell. We have modeled the cell using an average coat thickness of 0.15 μm, whereas the true particle has a thicker coat in the acrosomal region and a thin coat elsewhere.

The autocorrelation function obtained is not dependent on the speed input into the calculation but is very sensitive to the frequency of the oscillatory motion of the head of the spermatozoon. This means that it is only possible to get the frequency of the motion and not the speed, since the two are not related (Fig. 7). Furthermore, this work indicates that the point scattering interpretation made by Hallett et al. (1978) of the fitting parameter associated with Eq. 22, namely the speed, was incorrect. It is the oscillatory frequency of the head of the sperm that is measured by light scattering. One may determine this frequency by in essence calibrating the phenomenological Eq. 22 using Eq. 20.

The cinematographic results indicate that as the temperature gets higher the defective swimming motion of the spermatozoon becomes chaotic. This chaos does not allow the cell to progress as quickly as it should. This temperature effect indicates that the oscillatory motion is dominant over the progressive motion since it is affected more by temperature. The angular amplitude of its oscillation becomes larger and the frequency becomes smaller. This indicates that it must be able to move only at a fixed angular speed. One can understand this by noting that the frequency gives the number of cycles of the oscillations per second that are performed and the amplitude gives the size of these oscillations. If the oscillations become larger and the angular speed remains constant, fewer cycles may be performed per second or the frequency becomes lower.

Received for publication 4 March 1981 and in revised form 8 July 1981.

REFERENCES

Adam, M., A. Hamelin, P. Bergé, and M. Goffaux. 1969. Possibilité d'application de la technique de diffusion inélastique de la lumière à l'étude de la vitalité des spermatozoïdes de taureaux. *Ann. Biol. Anim. Biochim. Biophys.* 9:651–655.

Berne, B. J., and R. Nossal. 1974. Inelastic light scattering by large structured particles. *Biophys. J.* 14:865–880.

Chen, S.-H., M. Holz, and P. Tartaglia. 1977. Quasi-elastic light scattering from structured particles. *Appl. Opt.* 16:187–194.

Cooke, D., F. R. Hallett, and C. A. V. Barker. 1976. Motility evaluation of bull spermatozoa by photon correlation spectroscopy. *J. Mechanochem. Cell Motil.* 3:219–223.

Craig, T., F. R. Hallett, and B. Nickel. 1979. Quasi-elastic light-scattering spectra of swimming spermatozoa: Rotational and translational effects. *Biophys. J.* 28:457–472.

Craig, T., and F. R. Hallett. 1982. Half-width scaling of electric field autocorrelation functions from bull spermatozoa. *Biophys. J.* 38:71–78.

Dubois, M., P. Jouannet, P. Bergé, B. Volochine, C. Serres, and G. David. 1975. Méthode et appareillage de mesure objective de la mobilité des spermatozoïdes humains. *Ann. Phys. Biol. Med.* 9:19–41.

Hallett, F. R., T. Craig, and J. Marsh. 1978. Swimming speed distributions of bull spermatozoa as determined by quasi-elastic light scattering. *Biophys. J.* 21:203–216.

Holz, M., and S.-H. Chen. 1978. Rotational-translational models for interpretation of quasi-elastic light scattering spectra of motile bacteria. *Appl. Opt.* 17:3197–3204.

Kotlarchyk, M., S.-H. Chen, and S. Asano. 1979. Accuracy of RGD approximation for computing light scattering properties of diffusing and motile bacteria. *Appl. Opt.* 18:2470–2479.

Nossal, R. 1971. Spectral analysis of laser light scattering from motile microorganisms. *Biophys. J.* 4:341–354.

Rikmenspoel, R., G. van Herpen, and J. Eijkhout. 1960. Cinematographic observations of the movement of bull sperm cells. *Phys. Med. Biol.* 5:167–181.

Shimizu, H., and G. Matsumoto. 1980. Observation of flagellation of spermatozoa by depolarized laser light scattering. *Biophys. J.* 29:167–176.

van Duijn, Jr. C., and C. van Voorst. 1971. Precision measurements of dimensions, refractive index, and mass of bull spermatozoa in the living state. *Mikroscopie.* 27:142–167.